Plasma Chemistry and Plasma Processing (2021) 41:1381–1395
https://doi.org/10.1007/s11090-021-10183-6

ORIGINAL PAPER

The Production of Plasma Activated Water in Controlled Ambient Gases and its Impact on Cancer Cell Viability

Sirli Raud[1] · Jüri Raud[2] · Indrek Jõgi[2] · Carl-Thomas Piller[2] · Toomas Plank[2] · Rasmus Talviste[2] · Tambet Teesalu[1] · Eero Vasar[1]

Received: 21 November 2020 / Accepted: 18 May 2021 / Published online: 27 May 2021

Abstract
The present study investigated the effect of plasma-produced reactive oxygen (ROS) and nitrogen (RNS) species on cancer cell viability. Reactive species were generated in deionized water by using an atmospheric pressure Ar plasma jet within the controlled ambient gases (air, O_2 or N_2), which allowed the production of plasma-activated water containing only ROS (e.g. O_3, H_2O_2) or both ROS and RNS (e.g. H_2O_2, NO_2^-, NO_3^-). A considerable amount of H_2O_2 was produced in all ambient gases, and its generation rate was highest in N_2 and lowest in O_2. The latter was connected with a H_2O_2 precursor, OH, efficient quenching in O_2 ambient gas. Small quantities of NO_2^- were generated during short (< 5 min) plasma treatments in ambient air and N_2. The highest amount of NO_3^- was produced in N_2 ambient gas. Ozone was detected only in the case of O_2 environment. Cell viability studies were carried out by utilizing two cancer cell lines: 4T1 (breast cancer) and PPC-1 (prostate cancer). The results of the colorimetric succinate dehydrogenase activity assay showed that the studied cell lines had a similar sensitivity to the plasma activated medium. The impact of medium produced in the O_2 ambient environment was determined by H_2O_2 content. The equivalent amount of H_2O_2 in the plasma activated medium produced in the N_2 ambient environment caused an almost two-fold higher viability than in the case of the O_2 ambient gas. It is proposed that this was due to the cellular proliferation enhancing effect of NH_3.

Keywords Plasma treatment · Plasma activated medium · Cancer cell viability · Reactive oxygen and nitrogen species

Introduction

Cold atmospheric pressure plasmas can be used to generate various reactive oxygen (ROS) and reactive nitrogen species (RNS). These plasma-generated reactive oxygen and nitrogen species (RONS) have shown potential applicability in cancer therapy [1, 2]. In anti-cancer

✉ Sirli Raud
sirli.raud@ut.ee

[1] Institute of Biomedicine and Translational Medicine, University of Tartu, Ravila str. 19, 50411 Tartu, Estonia

[2] Institute of Physics, University of Tartu, W. Ostwaldi str. 1, 50411 Tartu, Estonia

studies, two different plasma treatment techniques have been applied- direct and indirect treatment [3]. In case of direct plasma treatment, cells in suspension are directly exposed to plasma. This results in the exposure of cells to newly generated RONS, and other plasma entailed effects such as electrons, UV radiation, electric field, higher plasma temperature [4]. In addition to long-lifetime RONS (O_3, H_2O_2, NO_2^-, NO_3^-), short-lifetime RONS (OH, NO, NO_2, $ONOO^-$, O, O_2^-) could also have a biological impact in direct treatment. In the case of indirect treatment prior to exposure to cells a liquid is treated with plasma to generate plasma-activated medium [5] (plasma activated medium is hereafter abbreviated as PAM, and it describes plasma treated cell growth medium or plasma activated water (PAW) added to a cell growth medium). Indirect treatment involves only long-lifetime RONS.

Despite extensive in vitro and in vivo studies [3, 6, 7] demonstrating the anti-cancer effect of plasma produced RONS, there is still no general consensus on the biological mechanism(s) and role of particular RONS in plasma treatment selectivity. It has been established that the diffusion of ROS into a cancer cell is facilitated when compared to their healthy counterparts due to an increased number of aquaporins (AQPs) and a lower level of cholesterol in the cancer cell's membrane [8–10]. Among different RONS, H_2O_2 is one of the key particles [5, 11, 12], and it is well known that even very small amounts of H_2O_2 could be cytotoxic [13]. The diffusion of H_2O_2 into the cell is determined by the expression of AQP 1, 3, 5, and 8 [14, 15]. Compared to the ROS, relatively little is known about the impact of RNS; although, the transport of several RNS into cell (through phospholipid bilayers) is found to be even easier than ROS e.g. H_2O_2 [16]. It seems that RNS (NO_2^- and NO_3^-) alone in the PAM has no effect on cell viability [17], while the simultaneous action of NO_2^- and H_2O_2 reduces cancer cell viability [12, 17, 18]. NO_3^- has been considered to have both cytotoxic [19] and non-cytotoxic effects [17].

The complexity of plasma and liquid phase chemistry complicates the specification of the role of particular RONS in the anti-cancer effect. The composition of RONS in the liquid depends on several factors, including the configuration and type of the plasma source, the plasma's parameters, and the composition of liquid used in the plasma treatment (e.g. water, cell culture medium) [20–25]. Plasma jet is a plasma source that is often used in plasma medicine for RONS production. Plasma jet is usually produced in a stream of noble gas inside a dielectric tube and it expands to ambient gas where plasma particles react with ambient gas molecules and form precursors of RONS, which can dissolve into the treated liquid. Experiments carried out in ambient air environment have demonstrated that cancer cell viability decreases with increasing treatment time/plasma power [11, 20, 24] and the decreasing distance between jet nozzle and water surface [26]. The treatment of liquids in the ambient air is the most commonly used, and the simplest way, to generate a wide variety of reactive species, because air contains ca 78% N_2, 21% O_2, and additionally a small amount of other gases like CO_2, H_2O, etc. PAM treated in ambient air always contains both ROS and RNS due to reactions with air particles. Controlled ambient gas (e.g. pure N_2, O_2 or their mixtures), on the other hand, broadens the range of variation in RONS composition. Thus, in principle, it is possible to completely avoid RNS production. The most common technique for controlling ambient gas composition is to use the flow of shielding gases separating the treatment zone from the ambient air [17, 27, 28]; however, it is technically challenging to completely shield the treated liquid from open air and, thus, air particles could still participate in RONS formation [17]. Another possibility to control plasma jet ambient gas composition is to use a reactor isolated from open air and filled with desired ambient gas [29]. Some of isolated reactors are vacuum compatible. The option to vacuum the system before plasma treatment enables furthermore decrease the content of impurity gases in the ambient gas [30]. Additionally, isolated reactors allow to control gas pressure

and dynamics above liquid surface during the plasma treatment and, thus, increase the reproducibility of the process.

Plasma treated liquid is produced by an indirect method on the basis of cell growth medium or less frequently distilled water. The anti-cancer effect of both PAW added to the cell growth medium and plasma treated cell growth medium has been reported to be similar [5]. The plasma treatment of water has a remarkably simpler liquid phase chemistry, and the number of different reactive particles is expected to be smaller in PAW. Thus, the interpretation of its biological impact should be more straightforward.

Besides RONS composition and concentration, there are several side effects that could influence biological impact of PAM and complicate the comparison between different experiments. In the case of indirect plasma treatment, one critical parameter is the post-manufacturing timespan of PAM prior to using it in biological tests. First of all, the chemical composition of PAM could change after the end of the plasma treatment, e.g. remarkable decrease of O_3, H_2O_2 and NO_2^- concentration in water have been observed during the post-manufacturing time [31, 32]. Secondly, the plasma treatment may increase the temperature of PAM. In this case it is necessary to cool PAM before cell treatment, because the temperature over 40 °C induces macromolecular changes, affects functions in cellular compartments and finally, it can lead to cell death [33]. Likewise, the plasma treatment could drastically change solution pH [24, 29] and this may also affect PAM toxicity.

The aim of the current study was to investigate RONS formation in PAW produced in well-defined ambient gases (N_2/O_2/air) and evaluate the influence of different ROS/RNS compositions on the viability of cancer cells. As our experimental setup allowed the production of PAW containing only ROS, or mixtures of ROS and RNS, it was possible to differentiate the biological impact of these species.

Materials and Methods

PAW Preparation

The production of PAW was carried out inside a hermetic chamber, Fig. 1.

The plasma jet used for PAW production was induced inside a quartz tube (inner diameter 1 mm) with the Kurt J. Lesker AT6 radiofrequency (RF) power supply at a

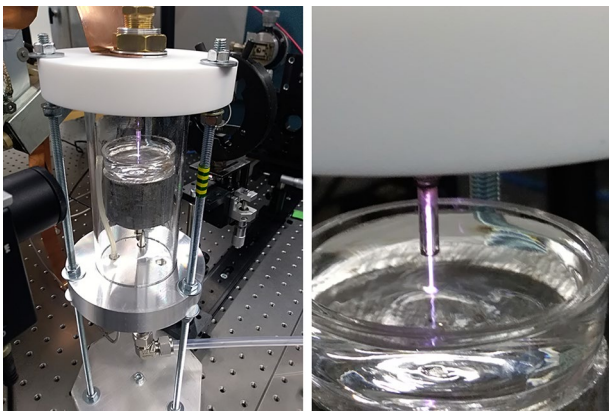

Fig. 1 Photos of PAW preparation in the isolated chamber. The Ar plasma jet expands from the quartz tube to ambient gas before reaching to the water surface. As a result of reactions between plasma particles, ambient gas, and water molecules, RONS will be formed in the water

frequency of 13.6 MHz. Most experiments were carried out at a generator output power of 50 W. The electrode connected to the RF power supply was formed by tightly wrapped wire around the tube placed at 10 mm upstream of the tube's nozzle. The width of the electrode was 30 mm. The surface of the plasma-treated deionized water (DI water) was approximately 5 mm downstream from the tube nozzle. The flow rates of gases were regulated by the Alicat Scientific mass flow controller. The flow rate of the Ar feed gas was 300 sccm (standard cube centimeter per minute). Some experiments were carried out in open air, while the influence of N_2 or O_2 ambient gas was studied in a chamber isolated from the open air. The flow rate of ambient gas was kept at 500 sccm. All experiments were conducted at atmospheric pressure. Before the experiments with the isolated chamber, the chamber was evacuated down to the base pressure of 0.02 Torr (to remove air particles from the feed and ambient gas tubes), and subsequently the desired gas flow rates were set. After this, the chamber was filled to 760 Torr and a Petri dish with DI water was placed inside the chamber. To minimize the content of air gases, the chamber was evacuated down to 100 Torr and filled to 850 Torr ten times. This procedure ensured that air particles were removed from both gas and liquid phases; this was confirmed in spectral measurements, where optical spectra registered outside the tube in O_2 ambient gas did not reveal N_2 bands, and NO_2^- and NO_3^- bands in the water absorption spectra were also missing. As the next step, the atmospheric pressure was set in the chamber, and water was kept in the established gas environment without plasma for 5 min. Finally, the plasma jet was ignited.

The plasma water treatment experiments occurred in contact mode [24], which was established on the basis of visual appearance (Fig. 1) and electrical characteristics. The electrical characteristics were recorded with the oscilloscope TDS-540B by using a 1:100 Tektronix voltage probe P5100 and a McPherson current monitor 6585. The phase shift φ, between i and u, was determined on the basis of oscillograms. The plasma power was calculated similarly as described in our earlier studies [34, 35] according to the formula $P = \frac{1}{T}\int_0^T i_p(t)u_p(t)\mathrm{d}t$. At 50 W output power of the RF power supply, the plasma power, measured 5 min after the discharge ignition, was ≈ 9 W; it was almost independent on the ambient gas utilized. The line-integrated argon metastable $1s_5$ state atoms' concentration, $n_m l_a$, near the water surface was determined by using a set of tunable diode laser absorption spectroscopy (TDLAS) Thorlabs TLK-L780M. Here n_m is the density of Ar $1s_5$ state atoms and l_a is the absorption path length.The stability of laser operation was checked with a Fabry–Perot interferometer Thorlabs SA-200. The laser light intensity passing through the plasma jet was registered with the photodetector Thorlabs APD110A2. The electron density and temperature near the water's surface were determined from Stark broadening of the hydrogen Hα line (656 nm) and Ar continuum radiation in the spectral range 350…650 nm as described in studies [36, 37]. The Hα line and the N_2 band at 380 nm (vibrational transition 0–2) used for gas temperature estimation were recorded using a MDR-23 spectrometer (experimentally determined instrumental full width at half maximum 0.06 nm). The gas temperature was estimated as described in our previous study [38]. For temperature estimation in the case of O_2 ambient gas, a small amount of N_2 (0.03%) was introduced into Ar feed gas. Ar continuum radiation was recorded with an Ocean Optics USB4000 spectrometer (spectral range 185…850 nm, resolution ≈ 1 nm). The relative spectral sensitivity of spectrometers was determined with an Ocean Optics DH-2000-Cal calibrated light source. The spatial resolution of spectral measurements was 0.5 mm.

PAW Characterization

The total amount of DI water used in the plasma treatment experiment was 12.2 mL. The treatment duration was varied from 0.5 to 30 min. The water mass and temperature were measured before and after the plasma treatment by balance Kern EG 220 3-NM and the infrared thermometer Meterman IR608, respectively. The temperature was estimated approximately one minute after the end of plasma treatment. 4 mL of PAW was used for RONS composition analysis, while the rest of PAW was used for cell viability tests and pH measurements. The pH of PAW was measured with the pH-meter SevenCompact S210. The analysis of RONS composition in PAW was performed within 3 min after the end of plasma treatment by using UV-absorption spectroscopy, as described in our previous work [24]. In brief, the absorption spectra, as recorded by the Ocean Optics USB4000 spectrometer, were fitted numerically with synthetic spectra, which were obtained from a linear combination of O_2, O_3, NO_2^-, NO_3^-, and H_2O_2 absorption spectra. For a determination of the O_3 absorption profile, DI water was treated with ozone produced by a homemade ozone generator, and O_3 concentration in water was calculated by using molar attenuation coefficient 5.2 mM^{-1} cm^{-1} at peak value of absorbance [39]. Examples of fitted experimental and synthetic spectra together with the absorption spectra of individual species are shown in Fig. 2.

Cell Viability Tests

PPC-1 prostate carcinoma cells and 4T1 breast cancer cells were cultured in DMEM (Life Technologies) and supplemented with 10% (v/v) fetal bovine serum (Atlantic Biologicals) and 1% (v/v) Penicillin and Streptomycin (Life Technologies) at 37 °C in a humidified incubator containing 5% (v/v) CO_2. 10,000 cells per well (200 µL/well) were seeded in 96-well flat-bottomed tissue culture-coated microplates (Falcon) followed by an overnight incubation. The medium was replaced with a fresh medium (100 µL medium/well), and freshly prepared PAW (or deionized water negative control) was added subsequently (100 µL/well). PAW was added to the cells within 3 min after the plasma treatment, with an initial 30 s reserved for PAW cooling. After incubation in the CO_2 incubator for 48 h, the cell viability was studied colorimetrically by using the 3-(4, 5-dimethylthiazol-2-yl)-2, 5-diphenyltetrazolium bromide (MTT) assay (Sigma-Aldrich) as described in our previous work [24].

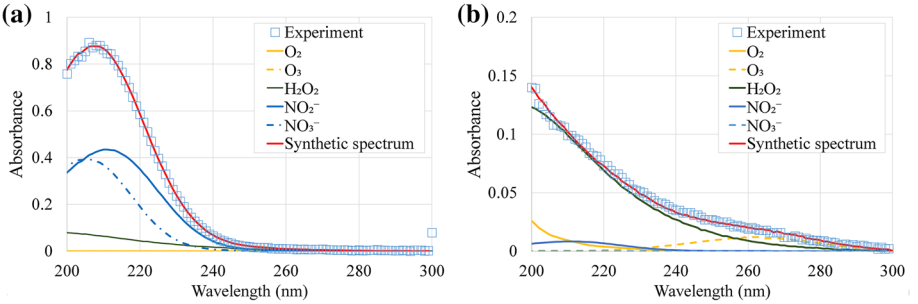

Fig. 2 Examples of experimental and synthetic spectra together with absorption spectra of individual species used in fitting in the case of (**a**) N_2 and (**b**) O_2 ambient gases

Uncertainty Estimation

Uncertainties shown in figures are of A-type at a confidence level of 90%. They were calculated from statistical standard deviation according to the formula $t\mathrm{stdev}/\sqrt{n}$, where t is the student coefficient and n is the number of repeated experiments.

Results and Discussion

PAW Temperature and Mass Loss

Figure 3 shows the PAW temperature and mass loss due to evaporation as a function of plasma treatment time.

Plasma treatment increased quickly the water temperature and it reached a stable level in ~ 7–10 min. The highest temperature, and mass loss due to evaporation, was observed in the case of N_2 environment and the lowest in the ambient air. The mass loss of PAW increased in time, and after the 30-min treatment, the mass loss ranged from 2.7 to 3.7 g. Using the vaporization heat of water at 50 °C, 2400 kJ/kg, the power transferred to the water (for evaporation of 3 g water for 30 min) is approximately half of the plasma power, 4 W. The considerable mass loss limited the time of plasma treatment and affected the concentration of the RONS in the PAW.

PAW pH

PAW pH decreased with plasma treatment time, and the decrease rate depended on ambient gas utilized, Fig. 4.

In the case of PAW production in N_2 containing ambient gases, the pH decrease is connected with formation of NO_2^- and NO_3^- [32, 39, 40]:

$$2NO_2 + H_2O \rightarrow NO_2^- + NO_3^- + 2H^+ \quad \text{(R1)}$$
$$NO + NO_2 + H_2O \rightarrow 2NO_2^- + 2H^+ \quad \text{(R2)}$$
$$HNO_2 \rightleftarrows H^+ + NO_2^-,\ \mathrm{pKa} = 3.4 \quad \text{(R3)}$$
$$HNO_3 \rightleftarrows H^+ + NO_3^-,\ \mathrm{pKa} < 0 \quad \text{(R4)}$$

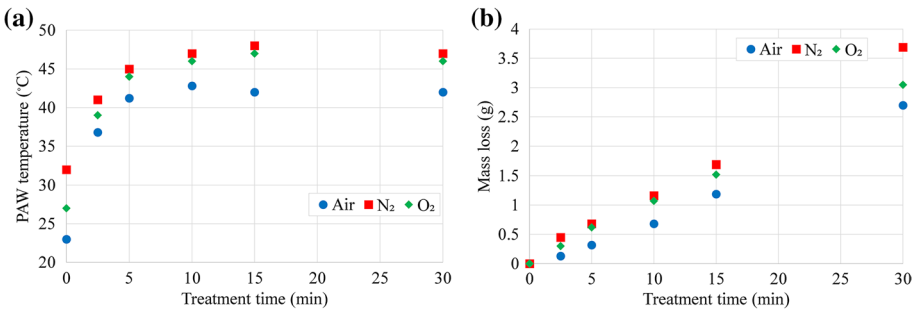

Fig. 3 Dependence of PAW temperature (**a**) and mass loss (**b**) on plasma treatment time. B-type uncertainties of temperature and mass loss determination were 2 °C and 0.2 mg, respectively

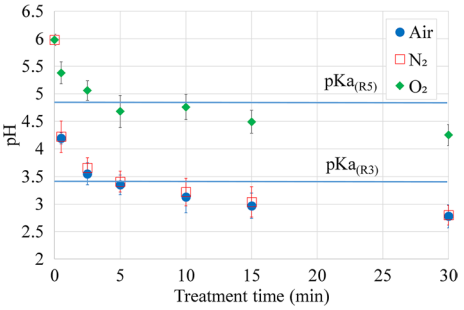

Fig. 4 The relationship between PAW pH and treatment time in the case of different ambient gases. The horizontal thick lines correspond to the pKa of reactions (R3, R5)

If PAW acidification is defined by reactions (R1-R4), then the sum of the concentration of anions $[NO_2^-]+[NO_3^-]$ should be equal to the concentration of protons. This equality was found, for example, in our previous work [24]. Nevertheless, with the concentrations of anions ("RONS composition of PAW"section, Fig. 5) and protons (calculated from pH, Fig. 4) in the present study, the ratio $([NO_2^-]+[NO_3^-])/[H^+]$ was larger than one. This suggests that some other cation besides H^+ should be present in PAW. One possible candidate is ammonium, NH_4^+, which has been found at relative high concentrations in water treated at O_2 deficient conditions [39, 41].

Compared with air or N_2, the pH decrease was smaller in the PAW produced in the O_2 environment. In an earlier study [42], the acidification of DI water in underwater plasma treatment (i.e. without N_2 presence) was explained with hydroperoxyl radical HO_2 deprotonation:

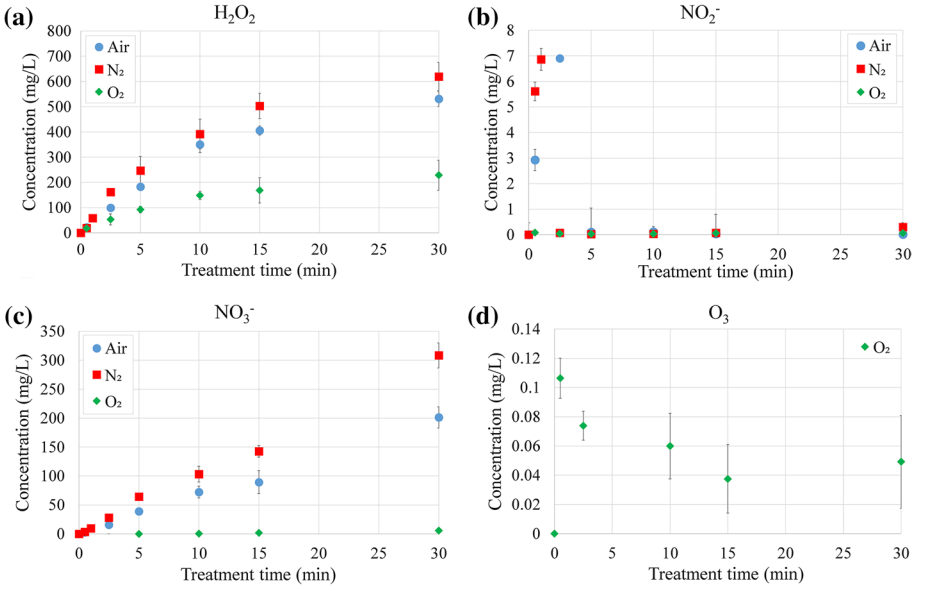

Fig. 5 Concentrations of H_2O_2 (**a**), NO_2^- (**b**), NO_3^- (**c**), O_3 (**d**) in PAW as a function of plasma treatment time for used ambient gases

$$HO_2 \rightleftarrows O_2^- + H^+ \quad (R5)$$

The pKa of this process is 4.8, which is close to the minimal pH value in the case of O_2 ambient gas.

RONS Composition of PAW

The production of long-lifetime RONS as a function of treatment time for used ambient gases is shown in Fig. 5.

The H_2O_2 concentration increased with treatment time. The highest H_2O_2 concentration was found in the case of the N_2 environment (≈600 mg/L) and lowest in the O_2 environment (≈250 mg/L). Similar trends in the dependence between H_2O_2 concentration and ambient gas during PAW production have been also observed in some earlier studies [17, 43]; however, there is no clear understanding in the mechanism(s) causing remarkably lower H_2O_2 concentration in the case of O_2 ambient gas. H_2O_2 forms in gas- or liquid phase [44–49] according to the reaction:

$$2OH + M \rightarrow H_2O_2 + M \quad (R6)$$

Assuming H_2O_2 formation in the gas phase, the rate constant of the reaction (R6) is k_{R6} ($M = N_2$) $= 1.4 \times 10^{-33}$ $cm^6 s^{-1}$ [50]. The gas temperature, necessary for the calculation of rate constant, $T_g \approx 1500$ K, was similar for both N_2 and O_2 ambient gases. According to data obtained from experiments at lower temperatures, the rate constants in N_2 and O_2 ambient gases are comparable [51, 52]. Independently from used ambient gas, H_2O_2 concentration was relatively stable in PAW; therefore, lower H_2O_2 concentration in the case of O_2 ambient gas could be connected with a lower concentration of its precursor, OH, in the gas phase– i.e. either the OH production rate is lower, or its quenching rate is higher in O_2 environment. OH radicals form from water vapor near the water surface [44, 53] mainly by H_2O dissociation by impact with Ar metastable state atoms or electrons [54, 55]. The lower H_2O_2 concentration in the case of O_2 ambient gas could not be due to a different amount of water vapor above the water surface as mass loss due to evaporation up to 15 min treatment durations is same in N_2 and O_2 ambient gases (Fig. 3b), H_2O_2 concentration, at the same time, is more than two times lower. According to our TDLAS measurements performed 1 mm from the water surface, a similar line integrated Ar metastable atom concentration ($n_m\, l_a \approx 2 \times 10^{14}$ m^{-2}) was presented in all used ambient gases. Assuming that the absorption path length, l_a is similar in all ambient gases, the OH production rate, through the H_2O dissociation by metastable Ar atoms, should be ambient gas independent. The rate of H_2O electron impact dissociation depends on electron concentration (n_e) and energy (T_e). Near the water surface (1 mm from the surface), n_e was highest in O_2 environment (6×10^{14} cm^{-3}) and lowest in N_2 (3×10^{14} cm^{-3}). In N_2 containing ambient gases, the reliable determination of T_e was possible only at distances > 2 mm from water surface. At 3 mm distances, $T_e \approx 0.5$ eV was similar in all ambient gases utilized. Thus, the electron impact production rate of OH should be highest in O_2 ambient gas due to higher n_e. Consequently, the notably lower H_2O_2 concentration in O_2 ambient gas should be the result of more efficient OH quenching. In O_2 ambient gas, OH could be quenched in the reaction with ozone [56]:

$$OH + O_3 \rightarrow HO_2 + O_2 \quad (R7)$$

At atmospheric pressure and gas temperature $T_g = 1500$ K, the rate constant of reaction (R7) is approximately three orders of magnitude larger ($k_{R7} = 6.3 \times 10^{-12}$ $cm^3 s^{-1}$

[57]) than (R6). Therefore, the quenching of OH in (R7) could be the reason for reduced H_2O_2 concentration in the case of ambient O_2. The maximum value of O_3 concentration in PAW, approximately 0.1 mg/L, was reached after 0.5 min of treatment. By using Henry´s law of solubility, the calculated O_3 concentration in the gas phase is $[O_3] = 1 \times 10^{15}$ cm^{-3} (Henry´s law coefficient for O_3, $H_{O3} = 1 \times 10^{-7}$ mol L^{-1} Pa^{-1} [58]) and the quenching frequency of OH in reaction (R7) is k_{R7} $[O_3] \approx 6 \times 10^3$ s^{-1}. Another effective OH quenching mechanism in ambient O_2 gas is the reaction with HO_2 [59]:

$$OH + HO_2 \rightarrow O_2 + H_2O \quad \text{(R8)}$$

At gas temperature 1500 K, the rate constant of reaction (R8) is $k_{R8} = 5.7 \times 10^{-11}$ cm^{3}s^{-1} [60]. At concentration $[HO_2] \sim 10^{14}$ cm^{-3}, found in the modeling study of Ar plasma jet water treatment [61], the quenching frequencies of OH in reactions (R7) and (R8) are similar. The quenching of OH by atomic oxygen could be also important in O_2 ambient gas as the rate constant of this reaction is high (2×10^{-11} cm^{3}s^{-1} [62].

At longer treatment times, the production rate of H_2O_2 was saturated (Fig. 5a). One possible reason for this saturation is that the distance between the plasma nozzle and water surface increased over time. The water loss due to evaporation reached up to ≈3 g after the 30-min plasma treatment (Fig. 3b), resulting in a ca 1 mm (i.e. 20%) distance increase.

NO_2^- and NO_3^- were detected in the PAW in the case of air and N_2 ambient gases (Fig. 5b, c). The concentration of the most abundant RNS, NO_3^-, increased with treatment time, and after 30 min plasma treatment reached up to 300 and 200 mg/L in the ambient N_2 and air, respectively. The NO_3^- concentration increase in time was almost linear; although, the distance between plasma nozzle and water surface increased. This may be due to the increased gas phase production of the NO_3^- precursor, NO_2 (reactions R1,R2), with the increase of distance [22]. The concentration of NO_2^- initially increased with treatment time and peaked after 1–2.5 min of plasma treatment up to ≈7 mg/L in both ambient N_2 and air. Further treatment caused the abrupt decrease of NO_2^- concentration down to zero. Both NO_2^- and NO_3^- are formed via reactions between plasma produced nitrogen oxide compounds and H_2O (R1, R2), and/or dissolved HNO_2 and HNO_3 in the water (R3, R4). The disappearance of NO_2^- after a few minutes of plasma treatment is possibly due to the fast acidification of PAW (Fig. 4), which causes the formation of HNO_2 by reaction (R3). The increase in H_2O_2 concentration during plasma treatment results in additional NO_2^- removal via reaction

$$NO_2^- + H_2O_2 + H^+ \rightarrow ONOOH + H_2O, \ \text{pKa} = 6.8 \quad \text{(R9)}$$

The product of reaction (R9), ONOOH, is mostly converted into HNO_3, and the latter dissociates according to reaction (R4) forming NO_3^- [32]. In order to estimate the importance of reaction (R9) in NO_2^- disappearance, we investigated the temporal dynamics of RONS concentration after 0.5 min of plasma treatment during the 60-min post treatment period in the case of N_2 ambient gas. The selected treatment duration ensured a relative high pH value (pH = 4.2)— the disappearance of NO_2^- in reaction (R3) was not important due to the remarkably lower pKa of this reaction. A slow and linear decrease in concentration was observed for NO_2^- (slope − 0.57 µM/minute, $R^2 = 0.83$) while NO_3^- concentration increased linearly (slope 0.40 µM/minute, $R^2 = 0.95$). The concentration of H_2O_2 remained relatively low after 0.5 min of plasma treatment (Fig. 5a), and we did not detect clear temporal trends for H_2O_2 concentration.

Cell Viability Tests

The viability decreased with plasma treatment time in the case of PAM containing ROS and RNS mixtures (PAW produced in ambient air and N_2) and only ROS (PAW produced in O_2 ambient) thus indicating that reduced cell viability was primarily caused by ROS and not RNS. Figure 6 shows cell viability's dependence on the concentration of the most abundant ROS, H_2O_2.

Both cell lines followed similar trends within margins of uncertainty. The viability decreased with an increase in H_2O_2 concentration, whereas the lowest viability at the given H_2O_2 was found for PAW produced in O_2 ambient gas. The PAW produced in O_2 ambient gas contained H_2O_2 and O_3 (Fig. 5d), and thus the lower viability found in O_2 ambient gas could be due to the presence of O_3. Moreover, according to a modelling study, O_3 transport through phospholipid bilayers is even more efficient than that of H_2O_2 [16]. However, in our experiments, O_3 concentration was relatively low and unlikely has an impact on cell viability as even several times higher O_3 concentration caused only a ~ 15% decrease in the viability of human colon carcinoma cells HT29 [63]. $^1O_2$ is another ROS which has been suggested to be important in cell viability and detected in plasma treated liquid, but its lifetime is too short to be important in the case of indirect treatment [64]. Thus, H_2O_2 was considered the main reactive compound in determining viability in our experiment. In order to check this assumption, H_2O_2 solutions with similar concentrations to that produced by plasma were made and added to cells (100 µL mixture of DI water and H_2O_2 was added to 100 µL DMEM containing cells). Equivalent quantities of H_2O_2 produced by plasma in O_2 ambient gas, or added directly to the cell growth medium, had the same effect on cell viability (Fig. 6). Therefore, we can conclude that the decrease of cell viability is determined mainly by H_2O_2. As referred to in the introduction section of this paper, the transport of H_2O_2 through the cell membrane depends on the expression of aquaporins 1, 3, 5, and 8. A similar sensitivity to H_2O_2 indicates on expression of these aquaporins in 4T1 and PPC-1 cell lines. We did not find studies concerning the expression of aquaporins in the utilized cell lines; however, there is indirect evidence that suggests that both cell lines possess these aquaporins. As a triple negative breast cancer cell line, 4T1 is expected to express aquaporins 3 and 5 [65]. While a study on similar prostate cell line, PC3 [66], suggests that in PPC-1, aquaporins 1, 3, and 5 are expressed.

PAW treated less than 2.5 min in ambient air or N_2 contained also NO_2^-, which acts synergistically with H_2O_2 to induce cell death [17, 18]. In our study, the NO_2^- concentration had a sharp maximum for plasma treatment after 0.5–1 min (Fig. 5b) but, within the

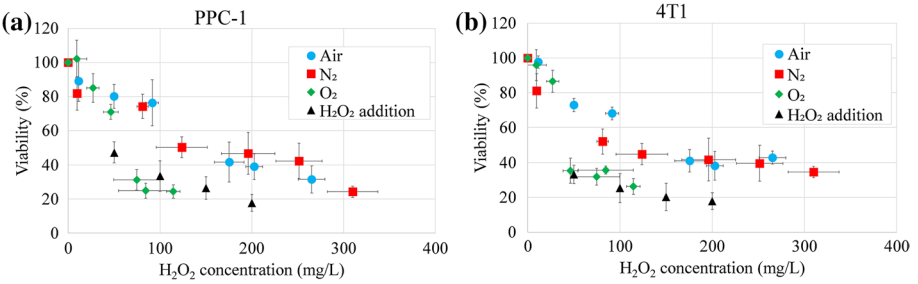

Fig. 6 Viability of PPC-1 (**a**) and 4T1 (**b**) cell lines as a function of H_2O_2 concentration. Note that H_2O_2 concentration is given by taking into account PAW dilution in DMEM (1:1)

margins of uncertainty, we did not detect a local minimum of viability for these treatments. We explain this result with the dominant impact of H_2O_2, which in our experiment exceeds NO_2^- concentration several times and probably masks the influence of NO_2^-.

Our results showed that RNS containing PAM had a smaller suppressive effect on viability than cell growth media where the equivalent amount of H_2O_2 was added, i.e. some nitrogen compounds alleviate the influence of H_2O_2. No such effect has been found for NO_2^- and NO_3^- [17]. From the disbalance between $[H^+]$ and $[NO_2^- + NO_3^-]$, we hypothesized that RNS-containing PAW may contain some other cation, likely NH_4^+. In this case, approximately 5% of total NH_3 and NH_4^+ exist in the liquid as NH_3 (calculated for 37 °C and pH 7.6 according to data given in [67]). It has been shown that ammonia can be incorporated in glutamine, an amino acid required for the growth and proliferation of cells [68]. This indirect pathway could explain the lower cytotoxicity of PAM containing RNS.

Besides the action of RONS, the decrease in cell viability could be due to side effects like DMEM acidification or an insufficient amount of nutrients after DMEM containing cells were mixed with PAW or DI water. To check whether the low pH of PAW influences the pH of cell growth media, the PAW with the lowest used pH (2.8) was added to DMEM in the same amount as in viability tests and pH was measured as a function of time. The addition of PAM to DMEM affected the pH of the mixture only slightly due to the presence of buffering agents in the DMEM (Fig. 7).

To check whether the amount of PAW/DI water in DMEM can influence cell viability results, we performed some additional cellular viability tests where the amount of PAW/DI water added to DMEM with cells (50 µL PAW/DI water to 150 µL DMEM) was smaller than in our main tests. We found that amount of PAW/DI water had no effect on viability since viability as a function of H_2O_2 concentration still coincided with the viability shown in Fig. 6 for 100 µL PAM/100 µL DMEM. A similar result was also obtained when we used PAM produced at lower generator power (40 W).

Summary and Conclusions

In our study, the influence of indirect plasma treatment on cancer cell viability was investigated. PAW was produced in different ambient gases (air, N_2 or O_2) by the atmospheric pressure RF argon plasma jet in contact mode. The concentrations of O_2, O_3, H_2O_2, NO_2^-, and NO_3^- in PAW were determined.

The use of different ambient gases during plasma treatment resulted in remarkable differences in RONS composition and concentration in PAW. The concentration of H_2O_2

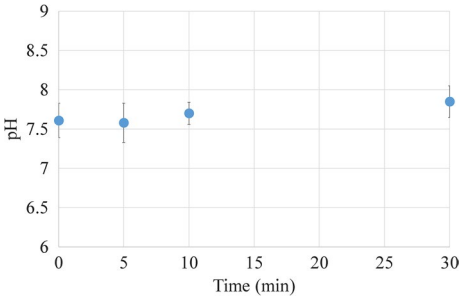

Fig. 7 Temporal dependence of pH after mixing 100 µL PAW (pH = 2.8) and 100 µL DMEM

increased with treatment time in all used ambient gases, whereas its production rate was highest in N_2 and lowest in O_2 ambient gas. A small amount of NO_2^- was detected in the case of N_2 containing ambient gases only after the first minutes of plasma treatment. The production rate of NO_3^- was almost constant in the ambient air and N_2, while its value was highest in N_2 ambient gas.

The application of PAM to cancer cell lines resulted in a decrease in cell viability. Two studied cancer cell lines– 4T1 (breast cancer) and PPC-1 (prostate cancer) – showed similar sensitivity to PAM treatment. The lowest cell viability was found in the case of O_2 ambient gas, and in this case the impact of PAM on cell viability could be explained solely by the effect of H_2O_2. The cell viability remained almost two times higher when PAM was produced in N_2 ambient gas or air, and this was explained through the proliferation enhancing effect of NH_3. The viability results were verified against possible PAW-associated side effects.

Acknowledgements The authors would like to thank Dr. Indrek Renge for valuable discussions on chemistry in the liquid phase. The present study was supported by Estonian Science Agency Grant no PUT1432.

Author contributions S.R., J.R. and I.J. contributed to the study conception and design. Experiments and data analysis were conducted by S.R., J.R. and C-T. P. S.R. wrote the manuscript with input from all authors.

Funding The study was supported by Estonian Science Agency Grant no PUT1432.

Declarations

Conflict of interest The authors have no conflicts of interest to declare that are relevant to the content of this article.

Data material The datasets generated during and/or analysed during the current study are available from the corresponding author on reasonable request.

References

1. Hirst AM, Frame FM, Arya M et al (2016) Low temperature plasmas as emerging cancer therapeutics: the state of play and thoughts for the future. Tumor Biology 37:7021–7031. https://doi.org/10.1007/s13277-016-4911-7
2. Semmler ML, Bekeschus S, Schäfer M et al (2020) Molecular mechanisms of the efficacy of Cold Atmospheric Pressure Plasma (CAP) in cancer treatment. Cancers 12:269
3. Canal C, Fontelo R, Hamouda I et al (2017) Plasma-induced selectivity in bone cancer cells death. Free Radic Biol Med 110:72–80. https://doi.org/10.1016/j.freeradbiomed.2017.05.023
4. Vandamme M, Robert E, Pesnel S et al (2010) Antitumor effect of plasma treatment on u87 glioma xenografts: preliminary results. Plasma Processes Polym 7:264–273. https://doi.org/10.1002/ppap.200900080
5. Kumar N, Attri P, Dewilde S, Bogaerts A (2018) Inactivation of human pancreatic ductal adenocarcinoma with atmospheric plasma treated media and water: a comparative study. J Phys D Appl Phys. https://doi.org/10.1088/1361-6463/aac571
6. Wang M, Holmes B, Cheng X et al (2013) Cold atmospheric plasma for selectively ablating metastatic breast cancer cells. PLoS ONE 8:e73741. https://doi.org/10.1371/journal.pone.0073741
7. Gerber IC, Mihai CT, Gorgan L et al (2017) Viability and cell biology for HeLa and vero cells after exposure to low-temperature air dielectric barrier discharge plasma. Plasma Med 7:159–173. https://doi.org/10.1615/PlasmaMed.2017019487
8. Van Der Paal J, Verheyen C, Neyts EC, Bogaerts A (2017) Hampering effect of cholesterol on the permeation of reactive oxygen species through phospholipids bilayer: possible explanation for plasma cancer selectivity. Sci Rep 7:1–11. https://doi.org/10.1038/srep39526

9. Yusupov M, Razzokov J, Cordeiro RM, Bogaerts A (2019) Transport of reactive oxygen and nitrogen species across aquaporin: a molecular level picture. Oxid Med Cell Longev. https://doi.org/10.1155/2019/2930504
10. Yan D, Xiao H, Zhu W et al (2017) The role of aquaporins in the anti-glioblastoma capacity of the cold plasma-stimulated medium. J Phys D Appl Phys. https://doi.org/10.1088/1361-6463/aa53d6
11. Bekeschus S, Lin A, Fridman A et al (2018) A comparison of floating-electrode DBD and kINPen jet: plasma parameters to achieve similar growth reduction in colon cancer cells under standardized conditions. Plasma Chem Plasma Process 38:1–12. https://doi.org/10.1007/s11090-017-9845-3
12. Dezest M, Chavatte L, Bourdens M et al (2017) Mechanistic insights into the impact of cold atmospheric pressure plasma on human epithelial cell lines. Sci Rep 7:1–17. https://doi.org/10.1038/srep41163
13. Gülden M, Jess A, Kammann J et al (2010) Free radical biology & medicine cytotoxic potency of H 2 O 2 in cell cultures : impact of cell concentration and exposure time. Free Radical Biol Med 49:1298–1305. https://doi.org/10.1016/j.freeradbiomed.2010.07.015
14. Bienert GP, Chaumont F (2014) Aquaporin-facilitated transmembrane diffusion of hydrogen peroxide. Biochim Biophys Acta Gen Subj 1840:1596–1604. https://doi.org/10.1016/j.bbagen.2013.09.017
15. Direito I, Madeira A, Brito MA, Soveral G (2016) Aquaporin-5: from structure to function and dysfunction in cancer. Cell Mol Life Sci 73:1623–1640. https://doi.org/10.1007/s00018-016-2142-0
16. Razzokov J, Yusupov M, Cordeiro RM, Bogaerts A (2018) Atomic scale understanding of the permeation of plasma species across native and oxidized membranes. J Phys D Appl Phys. https://doi.org/10.1088/1361-6463/aad524
17. Girard P-M, Arbabian A, Fleury M et al (2016) Synergistic effect of H2O2 and NO2 in cell death induced by cold atmospheric He plasma. Sci Rep 6:29098. https://doi.org/10.1038/srep29098
18. Bauer G, Sersenová D, Graves DB, Machala Z (2019) Dynamics of singlet oxygen-triggered, RONS-based apoptosis induction after treatment of tumor cells with cold atmospheric plasma or plasma-activated medium. Sci Rep 9:1–34. https://doi.org/10.1038/s41598-019-50329-3
19. Xu D, Cui Q, Xu Y et al (2018) NO_2^- and NO_3^- enhance cold atmospheric plasma induced cancer cell death by generation of $ONOO^-$. AIP Adv 8:105219. https://doi.org/10.1063/1.5046353
20. Cheng X, Sherman J, Murphy W et al (2014) The effect of tuning cold plasma composition on glioblastoma cell viability. PLoS ONE 9:1–9. https://doi.org/10.1371/journal.pone.0098652
21. Vermeylen S, De Waele J, Vanuytsel S et al (2016) Cold atmospheric plasma treatment of melanoma and glioblastoma cancer cells. Plasma Processes Polym 13:1195–1205. https://doi.org/10.1002/ppap.201600116
22. Uchida G, Nakajima A, Ito T et al (2016) Effects of nonthermal plasma jet irradiation on the selective production of H_2O_2 and NO_2^- in liquid water. J Appl Phys 120:203302. https://doi.org/10.1063/1.4968568
23. Jõgi I, Talviste R, Raud S et al (2020) Comparison of two cold atmospheric pressure plasma jet configurations in argon. Contrib Plasma Phys. https://doi.org/10.1002/ctpp.201900127
24. Talviste R, Raud S, Jogi I et al (2019) Investigation of a He micro plasma-jet utilized for treatment of prostate cancer cells. Plasma Res Express. https://doi.org/10.1088/2516-1067/ab4ea9
25. Kaushik NK, Ghimire B, Li Y et al (2019) Biological and medical applications of plasma-activated media, water and solutions. Biol Chem 400:39–62. https://doi.org/10.1515/hsz-2018-0226
26. Yan D, Talbot A, Nourmohammadi N et al (2015) Principles of using cold atmospheric plasma stimulated media for cancer treatment. Sci Rep 5:1–17. https://doi.org/10.1038/srep18339
27. Jablonowski H, Hänsch MACh, Dünnbier M et al (2015) Plasma jet's shielding gas impact on bacterial inactivation. Biointerphases 10:029506. https://doi.org/10.1116/1.4916533
28. Liu Z, Xu D, Liu D et al (2017) Production of simplex RNS and ROS by nanosecond pulse N2/O2 plasma jets with homogeneous shielding gas for inducing myeloma cell apoptosis. J Phys D Appl Phys. https://doi.org/10.1088/1361-6463/aa66f0
29. Azzariti A, Iacobazzi RM, Di Fonte R et al (2019) Plasma-activated medium triggers cell death and the presentation of immune activating danger signals in melanoma and pancreatic cancer cells. Sci Rep 9:1–13. https://doi.org/10.1038/s41598-019-40637-z
30. Lietz AM, Barnat EV, Foster JE, Kushner MJ (2020) Ionization wave propagation in a He plasma jet in a controlled gas environment. J Appl Phys. https://doi.org/10.1063/5.0020264
31. Noori H, Raud J, Talviste R, Jõgi I (2020) Water dissolution of nitrogen oxides produced by ozone oxidation of nitric oxide. Ozone: Sci Eng. https://doi.org/10.1080/01919512.2020.1839379
32. Lukes P, Dolezalova E, Sisrova I, Clupek M (2014) Aqueous-phase chemistry and bactericidal effects from an air discharge plasma in contact with water: Evidence for the formation of peroxynitrite through a pseudo-second-order post-discharge reaction of H2O2and HNO2. Plasma Sources Sci Technol. https://doi.org/10.1088/0963-0252/23/1/015019

33. Roti JL (2008) Cellular responses to hyperthermia (40–46°C): cell killing and molecular events. Int J Hyperth 24:3–15. https://doi.org/10.1080/02656730701769841
34. Jõgi I, Raud J, Hein K, Laan M (2014) Spectral characterization of medium-pressure RF discharge in argon-oxygen mixture. J Phys D Appl Phys. https://doi.org/10.1088/0022-3727/47/33/335206
35. Raud J, Jogi I, Matisen L et al (2017) Characterization of Ar/N2/H2 middle-pressure RF discharge and application of the afterglow region for nitridation of GaAs. J Phys D Appl Phys. https://doi.org/10.1088/1361-6463/aa9635
36. Yubero C, García MC, Calzada MD (2006) On the use of the Hα spectral line to determine the electron density in a microwave (2.45 GHz) plasma torch at atmospheric pressure. Spectrochim Acta - Part B Atomic Spectrosc 61:540–544. https://doi.org/10.1016/j.sab.2006.03.011
37. Park S, Choe W, Kim H, Park JY (2015) Continuum emission-based electron diagnostics for atmospheric pressure plasmas and characteristics of nanosecond-pulsed argon plasma jets. Plasma Sources Sci Technol. https://doi.org/10.1088/0963-0252/24/3/034003
38. Raud J, Laan M, Jgi I (2011) Rotational temperatures of N<inf>2</inf>(C,0) and OH(A,0) as gas temperature estimates in the middle pressure Ar/O<inf>2</inf> discharge. J Phys D Appl Phys. https://doi.org/10.1088/0022-3727/44/34/345201
39. Tachibana K, Nakamura T (2019) Comparative study of discharge schemes for production rates and ratios of reactive oxygen and nitrogen species in plasma activated water. J Phys D: Appl Phys. https://doi.org/10.1088/1361-6463/ab2529
40. Julák J, Hujacová A, Scholtz V et al (2018) Contribution to the chemistry of plasma-activated water. Plasma Phys Rep 44:125–136. https://doi.org/10.1134/S1063780X18010075
41. Kubota Y, Koga K, Ohno M, Hara T (2010) Synthesis of ammonia through direct chemical reactions between an atmospheric nitrogen plasma jet and a liquid. Plasma Fus Res 5:042–042. https://doi.org/10.1585/pfr.5.042
42. Royintarat T, Seesuriyachan P, Boonyawan D et al (2019) Mechanism and optimization of non-thermal plasma-activated water for bacterial inactivation by underwater plasma jet and delivery of reactive species underwater by cylindrical DBD plasma. Curr Appl Phys 19:1006–1014. https://doi.org/10.1016/j.cap.2019.05.020
43. Schmidt A, Bekeschus S, Jablonowski H et al (2017) Role of ambient gas composition on cold physical plasma-elicited cell signaling in keratinocytes. Biophys J 112:2397–2407. https://doi.org/10.1016/j.bpj.2017.04.030
44. He X, Lin J, Bangbang H et al (2018) The formation pathways of aqueous hydrogen peroxide in a plasma-liquid system with liquid as the cathode. Plasma Sources Sci Technol. https://doi.org/10.1140/epjd/e2020-100371-2
45. Gorbanev Y, O'Connell D, Chechik V (2016) Non-thermal plasma in contact with water: the origin of species. Chem Eur J 22:3496–3505. https://doi.org/10.1002/chem.201503771
46. Brisset JL, Hnatiuc E (2012) Peroxynitrite: a re-examination of the chemical properties of non-thermal discharges burning in air over aqueous solutions. Plasma Chem Plasma Process 32:655–674. https://doi.org/10.1007/s11090-012-9384-x
47. Brisset JL, Pawlat J (2016) Chemical effects of air plasma species on aqueous solutes in direct and delayed exposure modes: discharge, post-discharge and plasma activated water. Plasma Chem Plasma Process 36:355–381. https://doi.org/10.1007/s11090-015-9653-6
48. Tachibana K, Nakamura T (2019) Characterization of dielectric barrier discharges with water in correlation to productions of OH and H2O2 in gas and liquid phases. Jpn J Appl Phys. https://doi.org/10.7567/1347-4065/aafe73
49. Machala L, Tarabova B, Sersenova J, Hensel K (2019) Chemical and antibacterial effects of plasma activated water : correlation with gaseous and aqueous reactive oxygen and nitrogen species. J Phys D: Appl Phys 52:17
50. Sellevag SR, Georgievskii Y, Miller JA (2009) Kinetics of the gas-phase recombination reaction of hydroxyl radicals to form hydrogen peroxide. J Phys Chem A 113:4457–4467. https://doi.org/10.1021/jp8110524
51. Atkinson R, Baulch DL, Cox RA et al (1989) Evaluated kinetic and photochemical data for atmospheric chemistry: supplement III. IUPAC subcommittee on gas kinetic data evaluation for atmospheric chemistry. J Phys Chem Ref Data. https://doi.org/10.1063/1.555832
52. Atkinson R, Baulch DL, Cox RA et al (2004) Evaluated kinetic and photochemical data for atmospheric chemistry: part 1 – gas phase reactions of O_x, HO_x, NO_x and SO_x species. Atmos Chem Phys Discuss 3:6179–6699. https://doi.org/10.5194/acpd-3-6179-2003
53. Sasaki S, Honda R, Hokari Y et al (2016) Characterization of plasma-induced cell membrane permeabilization: Focus on OH radical distribution. J Phys D Appl Phys. https://doi.org/10.1088/0022-3727/49/33/334002

54. Liu Y, Tan Z, Chen X et al (2019) A Numerical investigation on the effects of water vapor on electron energy and oh production in atmospheric-pressure he/h2o and ar/h2o plasma jets. IEEE Trans Plasma Sci 47:1593–1604. https://doi.org/10.1109/TPS.2019.2896060
55. Srivastava N, Wang C (2011) Effects of water addition on OH radical generation and plasma properties in an atmospheric argon microwave plasma jet. J Appl Phys. https://doi.org/10.1063/1.3632970
56. Staehelin J, Buehler RE, Hoigne J (1984) Ozone decomposition in water studied by pulse radiolysis. 2. Hydroxyl and hydrogen tetroxide (HO4) as chain intermediates. J Phys Chem 88:5999–6004. https://doi.org/10.1021/j150668a051
57. Ju LP, Han KL, Varandas AJC (2007) Variational transition-state theory study of the atmospheric reaction OH + O3 → HO2 + O2. Int J Chem Kinet 39:148–153. https://doi.org/10.1002/kin.20226
58. Sander R (2015) Compilation of Henry's law constants (version 4.0) for water as solvent. Atmos Chem Phys 15:4399–4981
59. Schmidt-Bleker A, Bansemer R, Reuter S, Weltmann KD (2016) How to produce an NOx- instead of Ox-based chemistry with a cold atmospheric plasma jet. Plasma Processes Polym 13:1118–1125. https://doi.org/10.1002/ppap.201600062
60. Baulch DL, Cobos CJ, Cox RA et al (1992) Evaluated kinetic data for combustion modelling. J Phys Chem Ref Data. https://doi.org/10.1063/1.555908
61. Verlackt CCW, van Boxem W, Bogaerts A (2018) Transport and accumulation of plasma generated species in aqueous solution. Phys Chem Chem Phys 20:6845–6859. https://doi.org/10.1039/c7cp07593f
62. Shin KS, Michael JV (1991) Rate constants for the reactions H+O2→OH+O and D+O 2→OD+O over the temperature range 1085–2278 K by the laser photolysis-shock tube technique. J Chem Phys 95:262–273. https://doi.org/10.1063/1.461483
63. Simonetti V, Quagliariello V, Giustetto P et al (2017) Association of ozone with 5-fluorouracil and cisplatin in regulation of human colon cancer cell viability: in vitro anti-inflammatory properties of ozone in colon cancer cells exposed to lipopolysaccharides (Evidence-Based Complementary an. Evid-Based Complemen Altern Med. https://doi.org/10.1155/2017/7414083
64. Bekeschus S, Mueller A, Miller V et al (2017) Physical plasma elicits immunogenic cancer cell death and mitochondrial singlet oxygen. IEEE Trans Radiat Plasma Med Sci 2:138–146. https://doi.org/10.1109/trpms.2017.2766027
65. Zhu Z, Jiao L, Li T et al (2018) Expression of AQP3 and AQP5 as a prognostic marker in triple-negative breast cancer. Oncol Lett 16:2661–2667. https://doi.org/10.3892/ol.2018.8955
66. Bründl J, Wallinger S, Breyer J et al (2018) Expression, localisation and potential significance of aquaporins in benign and malignant human prostate tissue. BMC Urol 18:1–9. https://doi.org/10.1186/s12894-018-0391-y
67. Emerson K, Russo RC, Lund RE, Thurston RV (1975) Aqueous ammonia equilibrium calculations: effect of pH and temperature. J Fish Res Board Can 32:2379–2383. https://doi.org/10.1139/f75-274
68. Lie S, Wang T, Forbes B et al (2019) The ability to utilise ammonia as nitrogen source is cell type specific and intricately linked to GDH, AMPK and mTORC1. Sci Rep 9:1–15. https://doi.org/10.1038/s41598-018-37509-3